Variability and quasi-decadal changes in the methane budget over the period 2000-2012

Marielle Saunois[1], Philippe Bousquet[1], Ben Poulter[2], Anna Peregon[1], Philippe Ciais[1], Josep G. Canadell[3], Edward J. Dlugokencky[4], Giuseppe Etiope[5,6], David Bastviken[7], Sander Houweling[8,9], Greet Janssens-Maenhout[10], Francesco N. Tubiello[11], Simona Castaldi[12,13,14], Robert B. Jackson[15], Mihai Alexe[10], Vivek K. Arora[16], David J. Beerling[17], Peter Bergamaschi[10], Donald R. Blake[18], Gordon Brailsford[19], Lori Bruhwiler[4], Cyril Crevoisier[20], Patrick Crill[21], Kristofer Covey[22], Christian Frankenberg[23,24], Nicola Gedney[25], Lena Höglund-Isaksson[26], Misa Ishizawa[27], Akihiko Ito[27], Fortunat Joos[28], Heon-Sook Kim[27], Thomas Kleinen[29], Paul Krummel[30], Jean-François Lamarque[31], Ray Langenfelds[30], Robin Locatelli[1], Toshinobu Machida[27], Shamil Maksyutov[27], Joe R. Melton[32], Isamu Morino[33] Vaishali Naik[34], Simon O'Doherty[35], Frans-Jan W. Parmentier[36], Prabir K. Patra[37], Changhui Peng[38,39], Shushi Peng[1,40], Glen P. Peters[41], Isabelle Pison[1], Ronald Prinn[42], Michel Ramonet[1], William J. Riley[43], Makoto Saito[27], Monia Santini[14], Ronny Schroeder[44], Isobel J. Simpson[18], Renato Spahni[28], Atsushi Takizawa[45], Brett F. Thornton[22], Hanqin Tian[46], Yasunori Tohjima[27], Nicolas Viovy[1], Apostolos Voulgarakis[47], Ray Weiss[48], David J. Wilton[17], Andy Wiltshire[49], Doug Worthy[50], Debra Wunch[51], Xiyan Xu[43,52], Yukio Yoshida[27], Bowen Zhang[46], Zhen Zhang[2,53], and Qiuan Zhu[39].

[1]Laboratoire des Sciences du Climat et de l'Environnement, LSCE-IPSL (CEA-CNRS-UVSQ), Université Paris-Saclay 91191 Gif-sur-Yvette, France
[2]NASA Goddard Space Flight Center, Biospheric Science Laboratory, Greenbelt, MD 20771, USA
[3]Global Carbon Project, CSIRO Oceans and Atmosphere, Canberra, ACT 2601, Australia
[4]NOAA ESRL, 325 Broadway, Boulder, Colorado 80305, USA
[5]Istituto Nazionale di Geofisica e Vulcanologia, Sezione Roma 2, via V. Murata 605 00143 Roma
[6]Faculty of Environmental Science and Engineering, Babes Bolyai University, Cluj-Napoca, Romania.
[7]Department of Thematic Studies – Environmental Change, Linköping University, SE-581 83 Linköping, Sweden
[8]Netherlands Institute for Space Research (SRON), Sorbonnelaan 2, 3584 CA Utrecht, The Netherlands
[9]Institute for Marine and Atmospheric Research Sorbonnelaan 2, 3584 CA, Utrecht, The Netherlands
[10]European Commission Joint Research Centre, Ispra (Va), Italy
[11]Statistics Division, Food and Agriculture Organization of the United Nations (FAO), Viale delle Terme di Caracalla, Rome 00153, Italy
[12]Dipartimento di Scienze Ambientali, Biologiche e Farmaceutiche, Seconda Universita di Napoli, via Vivaldi 43, 81100 Caserta, Italy
[13]Far East Federal University (FEFU), Vladivostok, Russky Island, Russia
[14]Euro-Mediterranean Center on Climate Change, Via Augusto Imperatore 16, 73100 Lecce, Italy
[15]School of Earth, Energy & Environmental Sciences, Stanford University, Stanford, CA 94305-2210, USA
[16]Canadian Centre for Climate Modelling and Analysis, Climate Research Division, Environment and Climate Change Canada, Victoria, BC, V8W 2Y2, Canada
[17]Department of Animal and Plant Sciences, University of Sheffield, Sheffield S10 2TN, UK
[18]University of California Irvine, 570 Rowland Hall, Irvine, California 92697, USA
[19]National Institute of Water and Atmospheric Research, 301 Evans Bay Parade, Wellington, New Zealand
[20]Laboratoire de Météorologie Dynamique, LMD/IPSL, CNRS Ecole polytechnique, Université Paris-Saclay, 91120 Palaiseau, France
[21]Department of Geological Sciences and Bolin Centre for Climate Research, Svante Arrhenius väg 8, SE-106 91 Stockholm, Sweden
[22]School of Forestry and Environmental Studies, Yale University New Haven, CT 06511, USA
[23] California Institute of Technology, Geological and Planetary Sciences, Pasadena, USA
[24]Jet Propulsion Laboratory, M/S 183-601, 4800 Oak Grove Drive, Pasadena, CA 91109, USA
[25]Met Office Hadley Centre, Joint Centre for Hydrometeorological Research, Maclean Building, Wallingford OX10 8BB, UK
[26]Air Quality and Greenhouse Gases program (AIR), International Institute for Applied Systems Analysis (IIASA), A-2361 Laxenburg, Austria
[27]Center for Global Environmental Research, National Institute for Environmental Studies (NIES), Onogawa 16-2, Tsukuba, Ibaraki 305-8506, Japan
[28]Climate and Environmental Physics, Physics Institute and Oeschger Center for Climate Change Research, University of Bern, Sidlerstr. 5, CH-3012 Bern, Switzerland
[29]Max Planck Institute for Meteorology, Bundesstrasse 53, 20146 Hamburg, Germany
[30]CSIRO Oceans and Atmosphere, Aspendale, Victoria 3195 Australia

[31]NCAR, PO Box 3000, Boulder, Colorado 80307-3000, USA
[32]Climate Research Division, Environment and Climate Change Canada, Victoria, BC, V8W 2Y2, Canada
[33]Center for Global Environmental Research, National Institute for Environmental Studies (NIES), Onogawa 16-2, Tsukuba, Ibaraki 305-8506, Japan.
[34]NOAA, GFDL, 201 Forrestal Rd., Princeton, NJ 08540
[35]School of Chemistry, University of Bristol, Cantock's Close, Clifton, Bristol BS8 1TS
[36]Department of Arctic and Marine Biology, Faculty of Biosciences, Fisheries and Economics, UiT: The Arctic University of Norway, NO-9037, Tromsø, Norway
[37]Department of Environmental Geochemical Cycle Research and Institute of Arctic Climate and Environment Research, JAMSTEC, 3173-25 Showa-machi, Kanazawa-ku, Yokohama, 236-0001, Japan
[38]Department of Biology Sciences, Institute of Environment Science, University of Quebec at Montreal, Montreal, QC H3C 3P8, Canada
[39]State Key Laboratory of Soil Erosion and Dryland Farming on the Loess Plateau, Northwest A&F University, Yangling, Shaanxi 712100, China
[40]Sino-French Institute for Earth System Science, College of Urban and Environmental Sciences, Peking University, Beijing 100871, China
[41]CICERO Center for International Climate Research, Pb. 1129 Blindern, 0318 Oslo, Norway
[42]Massachusetts Institute of Technology (MIT), Building 54-1312, Cambridge, MA 02139, USA
[43]Earth Sciences Division, Lawrence Berkeley National Lab, 1 Cyclotron Road, Berkeley, CA 94720, USA
[44]Department of Civil & Environmental Engineering, University of New Hampshire, Durham, NH 03824, USA
[45]Japan Meteorological Agency (JMA), 1-3-4 Otemachi, Chiyoda-ku, Tokyo 100-8122, Japan
[46]International Center for Climate and Global Change Research, School of Forestry and Wildlife Sciences, Auburn University, 602 Duncan Drive, Auburn, AL 36849, USA
[47]Space & Atmospheric Physics, The Blackett Laboratory, Imperial College London, London SW7 2AZ, U.K.
[48]Scripps Institution of Oceanography (SIO), University of California San Diego, La Jolla, CA 92093, USA
[49]Met Office Hadley Centre, FitzRoy Road, Exeter, EX1 3PB, United Kingdom
[50]Environnement Canada, 4905, rue Dufferin, Toronto, Canada.
[51]Department of Physics, University of Toronto, 60 St. George Street, Toronto, Ontario, Canada
[52]CAS Key Laboratory of Regional Climate-Environment for Temperate East Asia, Institute of Atmospheric Physics, Chinese Academy of Sciences, Beijing 100029, China
[53]Swiss Federal Research Institute WSL, Birmensdorf 8059, Switzerland

Correspondance to: Marielle Saunois (marielle.saunois@lsce.ipsl.fr)

Supplementary material

1. Main characteristics of the individual top-down studies

Details on the individual inversions gathered for this study can be found in the referenced study in Table 1 of the main text. However we summarized here the components used as prior fluxes (Table S1) within each inversions as well as the treatment of the OH fields (TableS2).

Anthropogenic prior fluxes. All inversions use EDGAR inventory for the anthropogenic component of their prior fluxes. They differ in the versions used and how they handle the years following the ending date of the inventory (some uses the same values other update the values based on FAO and BP statistics (e.g., Houweling et al., 2014)). These anthropogenic emissions are provided as yearly value. Thus all modellers using EDGAR for the rice paddies emissions apply a seasonal cycle based on Matthews (1991) or Matthews and Fung (1987). GELCA, ACTM and NIESTM uses the surface land model VISIT-CH4 for rice paddies

Biomass burning prior fluxes. Most of the inversions use GFED3 estimates for biomass burning prior emissions.

Natural wetland prior fluxes. LMDz-PYVAR use the climatology from Kaplan (2002), not including inter annual variability. LMDz-MIOP uses either Kaplan (2002) or Matthews and Fung (1987), the latter including interannual variability. In this study the 10 inversions from LMDz-MIOP have been average to provide a single mean estimate. The TM5 based inversions uses estimate from the LPJ-WhyMe surface land model for natural wetland emissions while, ACTM, GELCA and NIEST-TM uses the estimates from VISIT-CH4. The methane emissions fluxes used are from previous run of both land models and differ from the runs performed for this study and Poulter et al. (2017), mostly because they do not use the same wetland area dataset.

Other natural prior fluxes. The inversions differ in the other than wetland natural sources. Most of the studies include termite and ocean emissions. Some may include other sources such as wild animal or geological seeps.

OH sink. In the top-down studies, the emission fluxes are optimized in order to match the atmospheric methane growth rate. However the methane growth rate results from the imbalance between sources and sinks. The main sink of methane is through its oxidation by the radical hydroxyl OH (e.g., Saunois et al., 2016). The amount of OH (and its distribution and variation) may impact the inferred methane fluxes for a given model both in magnitude and variations. Half of the models use the Transcom OH field from Spivakovsky et al. (2000) scaled to match the methane lifetime (Patra et al, 2011). OH concentrations were optimized with methylchloroform (MCF) observations (Table S2). The models using these data do not include interannual variability in OH concentrations. LMDz-PYVAR has a special treatment for OH. The prior OH fields are optimized using MCF observations during the inversions of methane fluxes, and corrected for 4 latitudinal bands at a weekly temporal scale. LMDZ-MIOP inversions include pre-optimized OH fields with IAV based on methyl chloroform observations.

Table S1. Components of the prior fluxes included in the individual top-down models.

Model	Anthropogenic other than rice	Rice	Biomass burning	Natural wetlands	Termites	Oceans	Other natural	Soil sink
CT-CH_4	EDGARv3.2FT2000	EDGARv3.2FT2000 following seasonal variations from Matthews (1991)	GFEDv3	Bergamaschi et al. (2005) based on Matthews (1995) and Kaplan (2002)	Sanderson (1996)	Lambert and Schmidt (1993) Houweling et al. (1999)	Wild animals (Houweling et al., 1999)	Ridgwell et al. (1999)
LMDZ-MIOP	EDGARv3.2	EDGARv3.2 following seasonal variations from Matthews and Fung (1987)	GFEDv2	Kaplan et al. (2002) or Matthews and Fung (1987)	Sanderson (1996)	Lambert and Schmidt (1993)	-	Ridgwell et al. (1999)
LMDZ-PYVAR	EDGARv4.2FT2010	EDGARv4.2FT2010 following seasonal variations from Matthews and Fung (1987)	GFEDv3.1	Kaplan et al. (2002)	Sanderson (1996)	Lambert and Schmidt (1993)		Ridgwell et al. (1999)
TM5 JRC	EDGARv4.2	EDGARv4.2FT2010 following seasonal variations from Matthews and Fung (1987)	GFEDv3.1	LPJ WHyMe (Spahni et al. 2011)	Sanderson (1996)	Lambert and Schmidt (1993)	Wild animals (Houweling et al., 1999)	Ridgwell et al. (1999)
TM5 SRON	EDGARv4.1	EDGARv4.1 following seasonal variations from Matthews and Fung (1987)	GFEDv3.1	LPJ WHyMe (Spahni et al. 2011)	Sanderson (1996)	Open oceans (Bates et al., 1996) Continental shelves (Kvenvolden and Rogers, 2005; Etiope and Klusman, 2002)	mud volcanoes, oil and gas Seeps (Houweling et al., 2014)	LPJ WHyMe (Spahni et al. 2011)
GELCA	EDGARv4.2FT2010	VISIT-CH4 (Ito and Inatomi, 2012)	GFEDv3.1	VISIT-CH4 (Ito and Inatomi, 2012)	Fung et al (1991)	-	-	VISIT-CH4 (Ito and Inatomi, 2012)
ACTM	EDGARv3.2	VISIT-CH4 (Ito and Inatomi, 2012)	GISS Fung et al (1991)	VISIT-CH4 (Ito and Inatomi, 2012)	GISS Fung et al (1991)	Lambert and Schmidt (1993)	mud volcano (Etiope and Milkov, 2004)	VISIT-CH4 (Ito and Inatomi, 2012)
NIES-TM	EDGARv4.2FT2010	VI VISIT-CH4SIT-CH4 (Ito and Inatomi, 2012)	GFEDv3.1	VISIT-CH4 (Ito and Inatomi, 2012)	Fung et al (1991)	-	-	VISIT-CH4 (Ito and Inatomi, 2012)

Table S2. List of the origin of the OH field for each individual top-down model.

Model	OH field origin	Inter annual variation (IAV)
CT-CH_4	Based on OH field from a TM5 full chemistry run; optimized using MCF	no IAV
LMDZ-MIOP	Prior OH Field from MOZART model (Hauglustaine 2004); optimized with MCF;	8 out of 10 inversions with IAV
LMDZ-PYVAR	Based on OH field from a LMDz-INCA full chemistry run;	no IAV in the prior fields; optimized with MCF during inversions
TM5 JRC	Based on OH field from a TM5 full chemistry run; optimized using MCF;	no IAV
TM5 SRON	From Transcom OH intercomparison (Patra et al., 2011)	no IAV
GELCA	From Transcom OH intercomparison (Patra et al., 2011)	no IAV
ACTM	From Transcom OH intercomparison (Patra et al., 2011)	no IAV
NIES-TM	From Transcom OH intercomparison (Patra et al., 2011)	no IAV

2. Variations in methane emissions inferred from inversions

Calculation of running means and running mean anomalies. The emission time series shown in Fig 1c of the main text (and similar plots in the supplementary) consist in 12-month running means calculated from the monthly fluxes provided by the modellers. As a result, the 6 first and last months were discarded. The associated anomaly (Fig. 1d) corresponds to the 12-month running means minus the mean over the full period of the runs. As a result the anomalies presented in Fig. 1d are relative to each inversion.
For studies providing numerous inversions (e.g., LMDz-MIOP), the mean of the time series were calculated and used throughout the text. In Fig. 1 c and d (and Fig. S2 to S5), the average estimate is plotted and the shaded area show the range between the minimum and maximum values inferred by the model (in grey for LMDz-MIOP).
In Fig. 2a, the mean anomaly corresponds to the average of the individual anomalies shown in Fig. 1d. The anomalies in Fig. 2b to 2f have been calculated the same way.

Year-to-year variations. Year-to-year variations as well as changes over some specific periods have been assessed for all individual inversions and summarized in Fig. S1. From 2004 to 2012, the year-to-year (year N minus year N-1) emission changes show some consistency between the inversions: for example lower emissions in 2009 associated with higher emissions in 2008 and 2010; quite stable emissions after in 2010-2012. Different periods were tested to assess the emissions change before and after 2007 (SP05-10, SP05-11; SP04-10). To limit the sensitivity to inter annual variability on the means, we decided to consider the difference between the average emissions over two 5-year periods: 2002-2006 and 2008-2012 (SP04-10 on fig. S1).

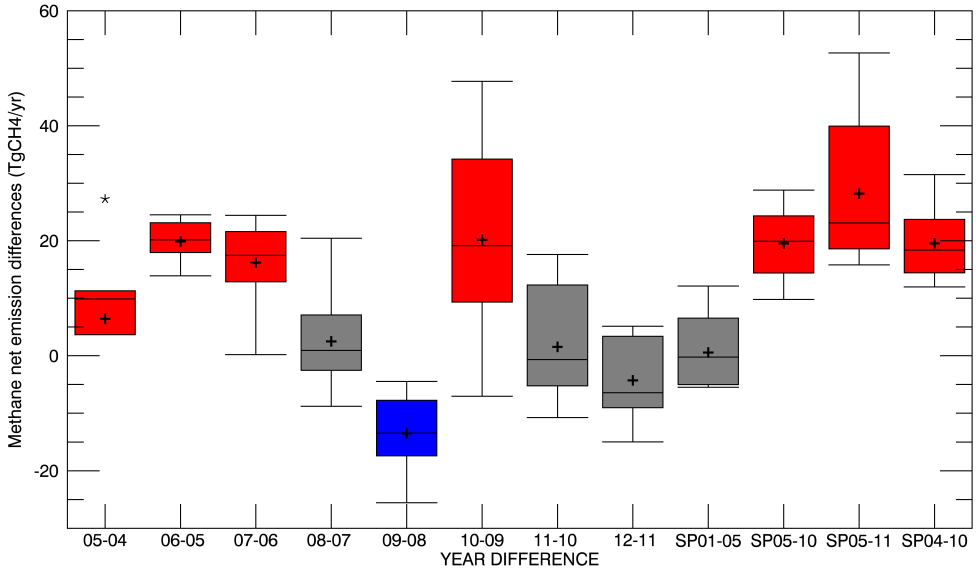

Figure S1: Box plots of the year to year differences in methane total emissions between 2004 and 2012 and differences between specific period (SP01-05 = year 2005 –year 2001; SP05-10= mean of (2009-2011) – mean of (2004-2006); SP05-11=mean of (2010-2012) – mean of (2004-2006); SP04-10=mean of (2008-2012) – mean of (2002-2006). Based on surface inversions only. Mean values are presented as + symbols, outliers as stars. In the main text we discuss the SP04-10, mean of (2008-2012) – mean of (2002-2006). Values are in Tg CH_4 yr^{-1}.

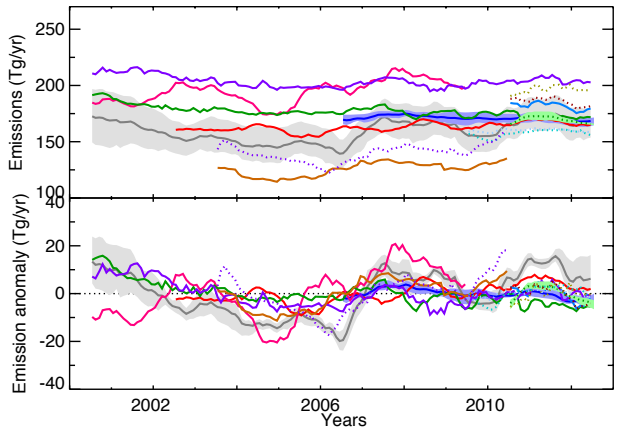

Figure S2: Emissions (top) and emission anomaly (bottom) of wetland emissions (Tg CH_4 yr^{-1}) inferred by the ensemble of inversions. The color scale is the same as for Figure 1 of the main manuscript.

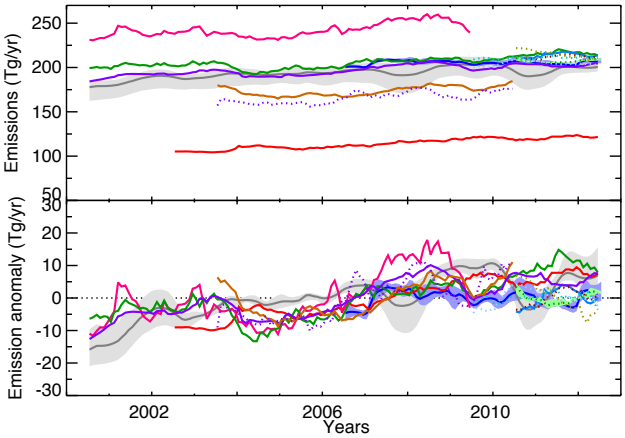

Figure S3: Same as Fig. S2 but for agriculture and waste emissions.

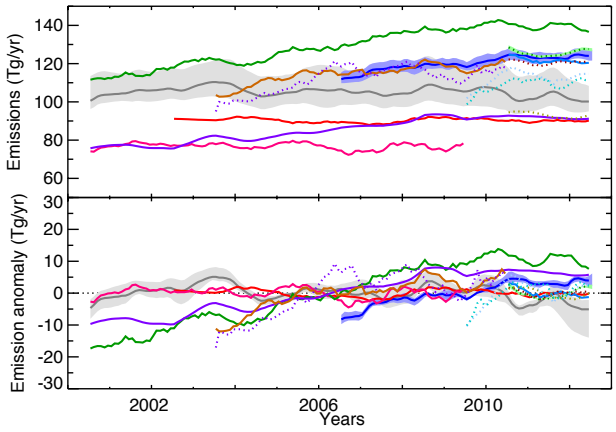

Figure S4: Same as Fig. S2 but for fossil fuel related methane emissions.

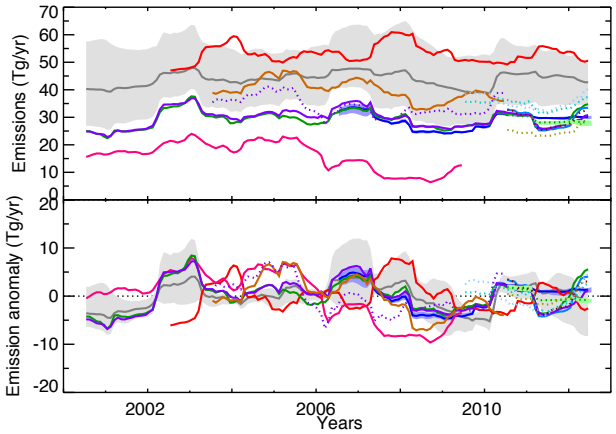

Figure S5: Same as Fig. S2 but for biomass burning and biofuel methane emissions.

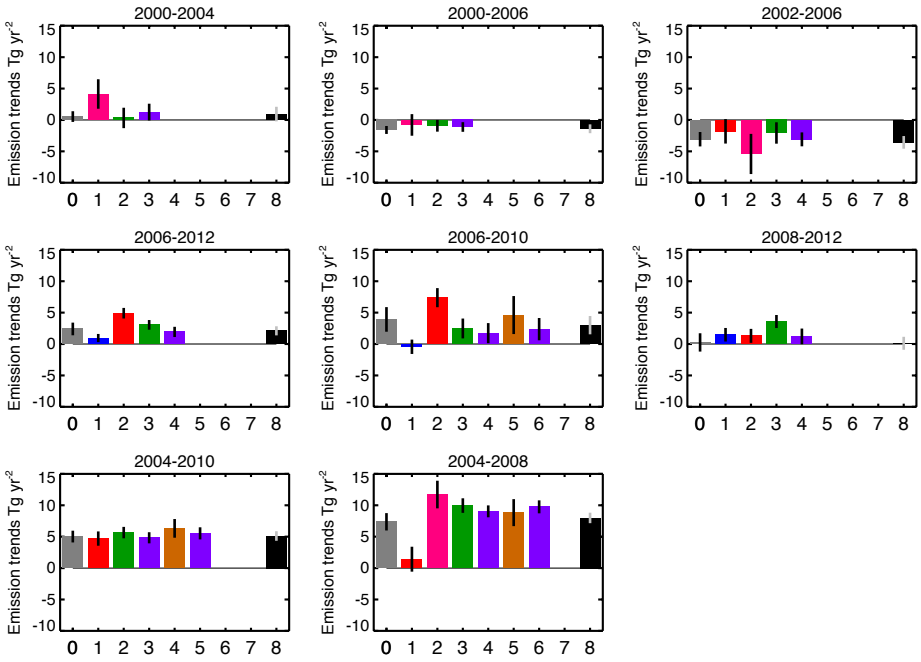

Figure S6: Methane emission trends calculated over eight different periods for the available top-down studies (coloured bars). Trends calculated based on the individual running means shown on Fig. 1. The colours of the bars correspond to the colours of the individual studies shown on Fig. 1. The upper right black bar corresponds to the trend calculated from the averaged anomaly shown on Fig. 2 (top-left). The error bar shows 2-sigma uncertainty on the calculated trend. The color scale is the same as for Figure 1 of the main manuscript.

3. Variations in methane emissions from bottom-up estimates

Time series for global fossil fuel, agriculture and waste emissions

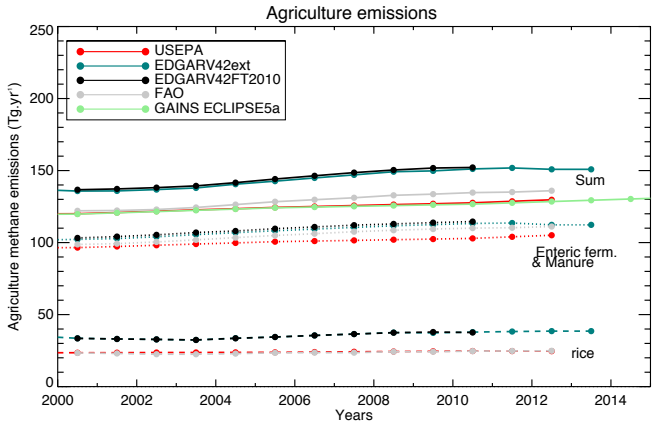

Figure S7: Methane yearly emissions from agriculture activities estimated by the inventories USEPA, EDGARv4.2, FAO and GAINS (Eclipse5a) in Tg CH_4 yr^{-1}. Rice in dashed lines, enteric fermentation and manure in dotted lines and the sum of both in solid lines.

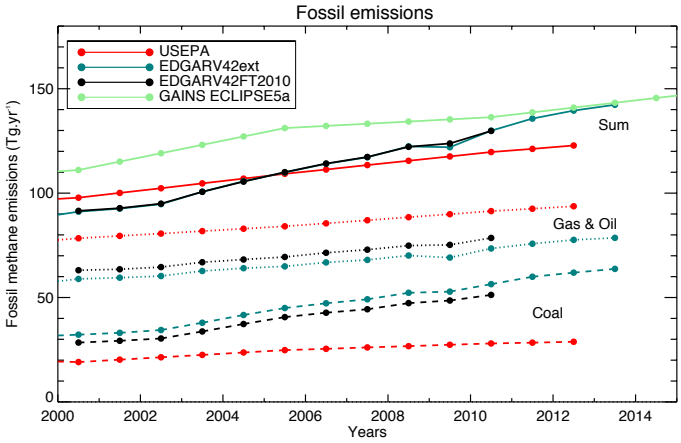

Figure S8: Methane yearly emissions from fossil fuel activities estimated by the inventories USEPA, EDGARv4.2, and GAINS (Eclipse5a) in Tg CH_4 yr^{-1}. Coal in dashed lines, Gas and Oil in dotted lines and the sum of both in solid lines.

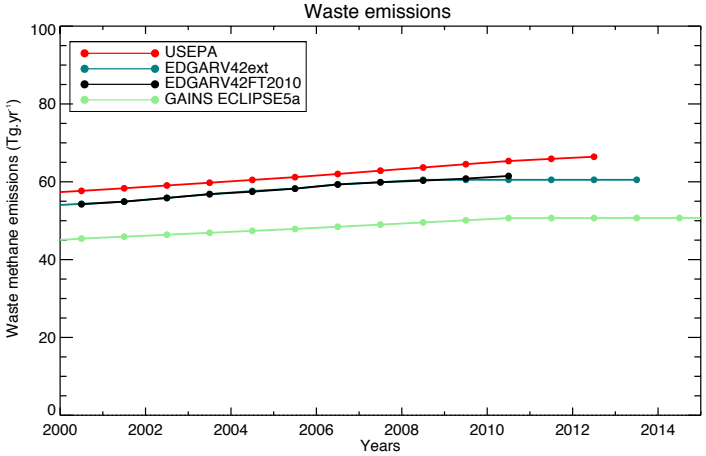

Figure S9: Methane yearly emissions from waste management activities estimated by the inventories USEPA, EDGARv4.2, and GAINS (Eclipse5a) in Tg CH_4 yr^{-1}.

Time series for global biomass burning emissions

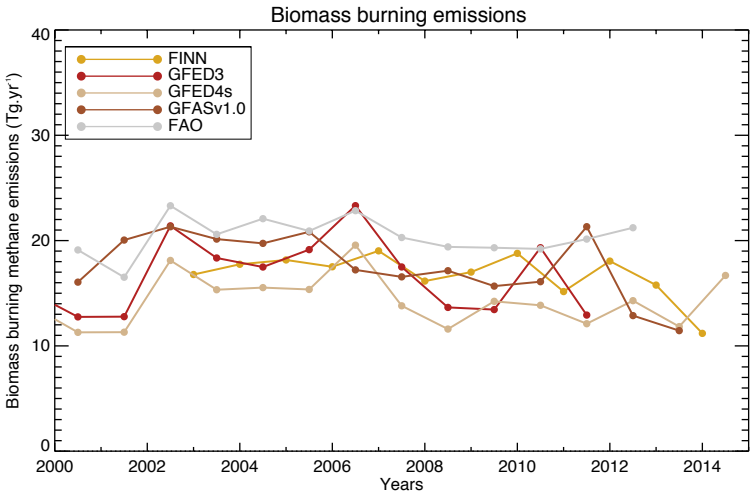

Figure S10: Methane yearly emissions from biomass burning estimated by FINN, GFED3, GFED4s, GFASv1.0 and FAO in Tg CH_4 yr^{-1}.

Time series for global wetland emissions

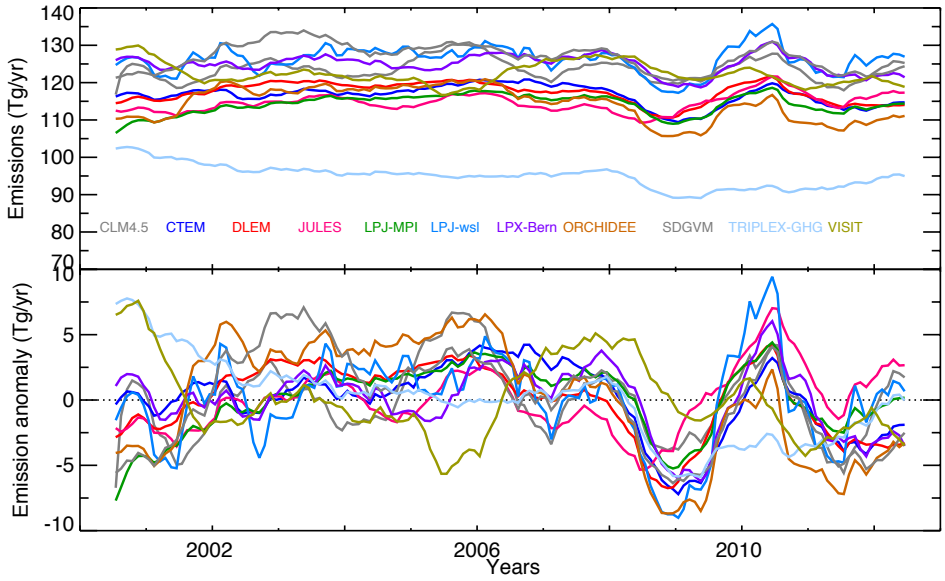

Figure S11: Emissions (top) and emission anomaly (bottom) from wetland (Tg CH_4 yr^{-1}) inferred by the 11 surface land models.

Time series for enteric fermentation from FAOSTAT

The FAOSTAT dataset used for the Global Methane Budget 2016 was downloaded on May 2016. This version is the one used Saunois et al. (2016) and in this study. There has been an update of this inventory (activity data) in September 2016, which has changed the methane emissions. Fig S12 and S13 show the methane emissions from agriculture based on the earlier version used so far and the updated one (to be used in future studies). The main change in this update is reduced cattle number in India, with a rather stable number since 2008. India is number one in agriculture methane emissions from enteric fermentation and manure. As a result, the update of Indian activity data impacts the global methane emission significantly.
The main differences between the two versions are the following:

1. Stable methane emission from agriculture in Asia in the newest version (Fig. S12)
2. Lower emissions but with the same trend in Africa, in particular
3. Lower global emissions over the 2000-2012 period with a weaker increasing rate after 2008 (FigS13), which is mainly due to the update in Indian activity data.

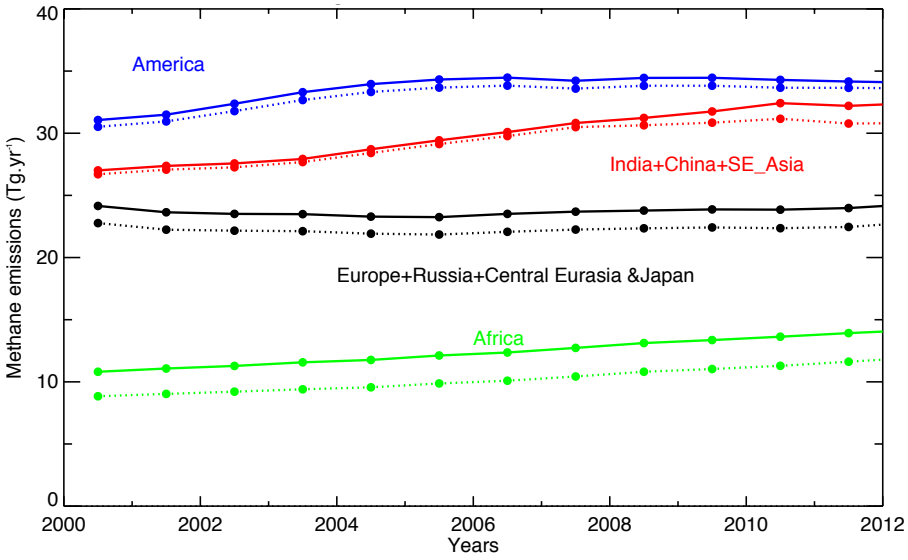

Figure S12: Emissions from enteric fermentation and manure (in Tg CH_4 yr^{-1}) over the four main continents: Africa, America, Asia (as China, India and South and East Asia), and the rest of Eurasia. Solid lines: the former version of FAOSTAT used in Saunois et al., 2016 and in this study. Dotted line: the updated (version of Jan. 2017) version of FAOSTAT.

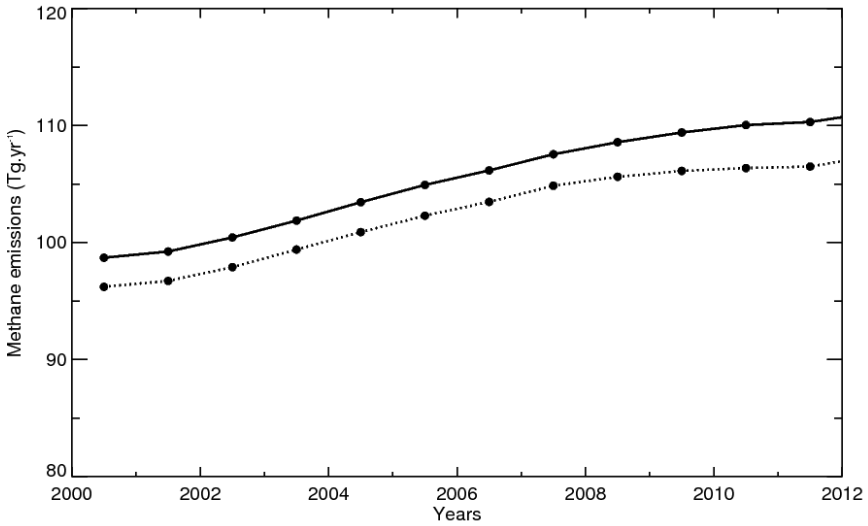

Figure S13: Global methane emissions from enteric fermentation and manure (in Tg CH_4 yr^{-1}). Solid lines: the former version of FAOSTAT used in Saunois et al., 2016 and in this study. Dotted line: the updated (version of Jan. 2017) version of FAOSTAT.

4. Emission change between 2002-2006 and 2008-2012

4.1 Inferred by top-down approaches

Table S3: Total methane emissions average the 2002-2006 period, the 2008-2012 period and differences in methane emissions between these two periods as derived by the individual top-down approaches. Values are in Tg CH_4 yr^{-1}.

	Average 02-06*	Average 08-12*	Difference**
Surface based inversions			
ACTM	540.2	564.8	24.6
CT-CH4[(a)]	563.0	-	15.3
GELCA	541.6	562.9	21.3
LMDzMIOP	530.0	546.3	16.5
LMDzPYVAR[(b)]	-	561.5	12.8
TM5 JRC	554.5	572.9	18.4
TM5 SRON[(c)]	544.3	567.1	22.8
NIESTM[(d)]	-		-
Satellite based inversions			
NIESTM[(d)]	-	572.0	-
TM5-JRC[(d)]	-	580.7	-
TM5 SRON[(d)]	-	579	-
TM5 SRON[(c)]	543.2	574.8	31.5
Average surface only	545.5	562.6	18.8
Average long runs only[(e)]	542.1	562.8	20.7
Average all	545.3	569.2	20.4

* a minimum of 3 years is required to calculate the average value over the 5-year periods
** no requirement is specified to calculate this difference
(a) ends in 2009; (b) starts in 2006; (c) starts in 2003 and ends in 2010, the satellite study is based on SCIAMACHY data
(d) starts in 2010, satellite studies are based on GOSAT data; (e) surface only, covering at least 3 years for each period, i.e. 5 studies (SCIAMACHY run is excluded)

Table S4: Changes in methane emissions (in Tg CH_4 yr^{-1}) between the 2002-2006 and 2008-2012 periods as derived by the individual top-down approaches. The associated average isotopic signature (in ‰) have been calculated based on Equation 1 and the isotopic signature from Schaefer et al. (2016) with a -49‰ signature for the "other natural" sources. Averages over inversions are made using different sets of inversions.

	Wetlands	Agriculture & Waste	Fossil fuels	Biomass burning	Other natural	Total emissions change	Average isotopic signature of the source change
ACTM	5.4	11.8	0.1	-0.1	7.4	24.6	-56.7
CT-CH4[(a)]	10.8	9.4	1.5	-9.1	2.7	15.3	-78.5
GELCA	-4.1	11.9	15.7	-2.2	1.1	22.4	-47.1
LMDzMIOP	16.2	6.8	-1.9	-2.2	-2.5	16.5	-69.3
LMDzPYVAR[(b)]	1.2	4.9	10.1	-4.2	0.5	12.6	-53.6
TM5 JRC	1.5	9.8	10.3	-4.0	0.9	18.4	-54.9
TM5 SRON[(c)]	8.2	9.7	8.4	-6.5	3.1	22.8	-60.9
SCIAMACHY TM5 SRON[(c)]	10.1	11.5	8.7	-2.1	3.4	31.5	-55.1
Average							
All inversions (8)	6.2	9.5	6.6	-3.8	2.1	20.5	-59.5
Only surface inversions (7)	5.6	9.2	6.3	-4.0	1.9	18.9	-60.2
Only long surface inversions (5)	5.5	10.0	6.5	-3.0	2.0	21.0	-57.8

(a) ends in 2009; (b) starts in 2006; (c) starts in 2003 and ends in 2010, the satellite study is based on SCIAMACHY data

4.2 Inferred by bottom-up approaches

Table S5: Methane emissions average the 2002-2006 period, the 2008-2012 period and differences in methane emissions between these two periods as estimated by inventories and biomass burning remote sensed estimates. Values are in Tg CH_4 yr^{-1}. Agriculture include enteric fermentation and manure management and rice cultivation. Fossil fuels include coal, oil and gas.

	Average 2002-2006 *	Average 2008-2012 *	Difference **
Agriculture (all activities)			
EDGARv4.2FT2010***	141.9	151.4	9.5
EDGARv4.2EXT	140.6	150.6	10.0
FAOSTAT	126.4	134.4	8.0
GAINS	123.2	126.9	3.7
USEPA	123.5	127.9	4.4
Enteric fermentation & Manure management			
EDGARv4.2FT2010***	108.2	113.8	5.6
EDGARv4.2EXT	106.8	112.7	5.9
FAOSTAT	103.4	109.9	6.5
USEPA	99.7	103.3	3.6
Rice cultivation			
EDGARv4.2FT2010***	33.7	37.6	3.9
EDGARv4.2EXT	33.8	37.9	5.9
FAOSTAT	23.0	24.5	1.6
USEPA	23.8	24.6	0.8
Fossil fuels			
EDGARv4.2FT2010***	105.1	125.2	20.2
EDGARv4.2EXT	105.0	129.9	24.9
GAINS	126.5	137.1	10.6
USEPA	106.9	119.3	12.4
Coal			
EDGARv4.2FT2010***	37.0	49.0	12.1
EDGARv4.2EXT	41.2	56.7	15.4
USEPA	23.6	27.9	4.3
Gas & Oil			
EDGARv4.2FT2010***	68.1	76.2	8.1
EDGARv4.2EXT	63.8	73.2	9.5
USEPA	83.0	91.2	8.2
Waste Management			
EDGARv4.2FT2010***	57.5	60.9	3.3
EDGARv4.2EXT	57.6	60.5	2.9
GAINS	47.4	50.3	2.9
USEPA	60.5	65.2	4.7
Biomass burning			
FAOSTAT	22.0	19.9	-2.1
FINN	17.8	16.8	-0.5
GFASv1.0	19.9	16.6	-3.2
GFED3	19.9	14.8	-5.1
GFED4s	16.8	13.2	-3.6

* a minimum of 3 years is required to calculate the average value over the 5-year periods

** no requirement is specified to calculate this difference

*** Note that EDGARv4.2FT2010 ends in 2010

Table S6: Methane emissions from wetlands average the 2002-2006 period, the 2008-2012 period and differences in methane emissions between these two periods as estimated by eleven surface land models. Values are in Tg CH_4 yr^{-1}.

	Average 2002-2006	Average 2008-2012	Difference
CLM4.5	207.4	206.4	-1.0
CTEM	196.0	194.3	-1.7
DLEM	170.4	165.7	-4.7
JULES	187.8	195.1	7.3
LPJ-MPI	224.9	227.3	2.5
LPJ-WSL	153.4	152.1	-1.2
LPX-Bern	174.0	173.0	-1.0
ORCHIDEE	177.1	169.0	-8.1
SDGVM	192.3	189.6	-2.7
TRIPLEX-GHG	155.4	153.0	-2.4
VISIT	193.7	197.4	3.7

Table S7: Wetland methane emission change between the 2002-2006 period and the 2008-2012 period as estimated by eleven surface land models for the southern hemisphere and tropics, the northern mid-latitudes and the boreal regions. Values are in Tg CH_4 yr^{-1}.

	90°S-30°N	30°-60°N	60°-90°N	Global
CLM4.5	-2.1	1.0	0.2	-1.0
CTEM	-3.6	1.7	0.3	-1.7
DLEM	-4.2	-0.6	0.0	-4.7
JULES	0.3	5.3	1.7	7.3
LPJ-MPI	-2.0	3.5	1.0	2.5
LPJ-WSL	-2.4	0.9	0.3	-1.3
LPX-Bern	-2.0	0.7	0.3	-1.0
ORCHIDEE	-8.3	-0.1	0.3	-8.1
SDGVM	-5.3	1.6	1.0	-2.7
TRIPLEX-GHG	-3.3	0.9	0.0	-2.4
VISIT	0.0	3.1	0.6	3.7
Average estimate	*-3.0*	*1.6*	*0.5*	*-0.9*

5. Update of EDGARv4.2 to EDGARv4.3.2

A revised version of EDGAR (EDGARv4.3.2) is soon to be released. In particular, this revised version uses region-specific emission factors in China. The consequences are both a decrease in the absolute emission in year 2000 and a lower increasing rate of coal methane emissions (Fig S14). Greet Maenhout has provided these partial data on a personal communication basis. The full data set wil be released on the EDGAR website soon and wil be associated to an article in ESSD (Janssens-Maenhout, G. Muntean, M., Crippa, M., Guizzardi, D., Schaaf, E., Dentener, F., Bergamschi, P., Pagliari, V., Olivier, J.G.J., Peters, J.A.H.W., van Aardenne, J.A., Monni, S., Doering, U., Petrescu, A.M.R., The 1970-2012 emissions atlas of EDGARv4.3.2: Part I - Greenhouse gas emissions, to be submitted to ESSD.)

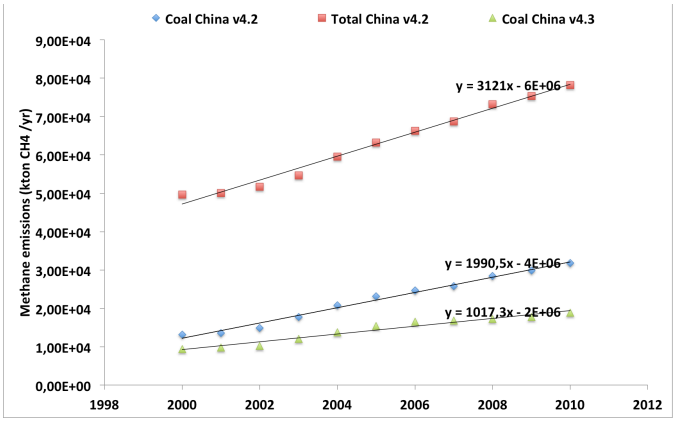

Figure S14: Chinese emissions extracted from EDGARv4.2FT2010 release (total in red and coal in blue) and the next version to be released EDGARv4.3.2 (only coal emissions in green) between 2000 and 2010. The linear trend and their equations are also shown.

6. Isoflux calculations

In the discussion section of the main text, the average isotopic signatures of the emission change have been calculated using two sets of mean isotopic signature for the main sources and presented in Fig. 6. The deviations of most of the individual inversions from the ensemble mean, in terms of average isotopic signature of the emission change between 2002-2006 and 2008-2012, highlight the sensitivity of the atmospheric isotopic signal to the changes in methane sources (Fig. 5 and Table S4). Another example of this sensitivity is illustrated by Schwietzke et al. (2016) who quantified the impact of uncertain biomass burning and fossil fuel isotopic signature trends on the trend in fossil fuel methane emissions. In a scenario assuming constant biomass burning emissions, fossil fuel emissions decrease; while in a scenario assuming decreasing biomass burning emissions, fossil fuel emissions remain constant.

The mean global source signature in $\delta^{13}C\text{-}CH_4$ is about -52‰. An average decrease of biomass burning emissions of about 3 Tg CH_4 yr^{-1} at -22‰ leads to a departure of (52-22)*3=90 Tg CH_4 yr^{-1} ‰ isoflux (isotopically weighted flux). This is equivalent to a (52-44)*11= 88 Tg CH_4 yr^{-1} ‰ isoflux, representing a 11 Tg CH_4 yr^{-1} decrease in fossil fuel emissions (isotopic signature of -44‰). Thus a larger decrease in biomass burning (of about 3 Tg CH_4 yr^{-1} as found here) could (isotopically) compensate an increase in fossil fuel related emissions and be consistent with atmospheric changes of both $^{12}CH_4$ and $^{13}CH_4$. These simple analyses show that apparently small variations of a source having an isotopic signature very different from the global mean isotopic source signature (δ^{13}_{source}=-52 ‰) needs to be considered as important as large changes of a source whose isotopic signature is closer to -52 ‰.